Materials Advances

ROYAL SOCIETY OF CHEMISTRY

PAPER

View Article Online
View Journal | View Issue

Check for updates

Cite this: *Mater. Adv.*, 2025, 6, 5523

Design strategies for liquid-phase synthesis of sodium-based quaternary solid-state electrolytes†

Saeed Ahmadi Vaselabadi,* Brynn Benham and Colin A. Wolden

Received 24th March 2025,
Accepted 1st July 2025

DOI: 10.1039/d5ma00270b

rsc.li/materials-advances

The cost-effective and scalable production of solid-state electrolytes is essential for advancing all-solid-state sodium batteries as a safer, lower-cost alternative to Li-ion batteries. Herein, we explored liquid-phase synthesis methods for quaternary chalcogenide solid-state electrolytes (SSEs) with the formula $Na_{11}Sn_2PnCh_{12}$ (Pn = P, Sb, Ch = S, Se). We outline the key design principles, including reagent selection, solvent chemistry, and thermal treatment, while elucidating reaction mechanisms through systematic studies using XRD, Raman, and FTIR spectroscopy. We demonstrate that acetonitrile, an aprotic solvent with high polarity, enables the synthesis of $Na_{11}Sn_2PS_{12}$ *via* a simple solution process followed by heat-treatment, achieving high ionic conductivity (σ_{Na^+} = 0.2 mS cm^{-1}). The antimony analog, $Na_{11}Sn_2SbS_{12}$, can be produced in an aqueous solution facilitated by reactive bisulfide intermediates, yielding a highly crystalline chalcogenide at low temperatures with excellent transport properties (σ_{Na^+} = 0.4 mS cm^{-1}). For selenide analogs (*e.g.* $Na_{11}Sn_2SbSe_{12}$), alkahest amine–thiol solvents facilitate synthesis from elemental and binary precursors, marking the first report of its kind. Additionally, we identified $Na_{11}Sn_2SbS_{12}$ as the most promising candidate for utilization in sodium all-solid-state batteries owing to its wide electrochemical stability and strong compatibility with Na–Sn alloy anodes.

Open Access Article. Published on 02 July 2025. Downloaded on 5/21/2026 10:57:09 PM.
This article is licensed under a Creative Commons Attribution-NonCommercial 3.0 Unported Licence.

Introduction

Solid-state sodium-ion batteries are attractive candidates to facilitate renewable energy integration due to sodium's abundance, low cost, and reduced environmental impact relative to their high-performance lithium counterparts. Sodium's relatively low atomic weight and its similar electrochemical potential make it a promising target for "post-Li" chemistry. Moreover, substitution of solid-state electrolytes for conventional organic liquid electrolytes can enhance energy density and specific capacity of the cell while mitigating flammability safety concerns. Sodium-based chalcogenides are promising candidates to realize sodium all-solid-state batteries owing to their high ionic conductivity (>0.1 mS cm^{-1}), favorable interfacial contact with electrodes based on their deformability, and mild processing requirements.[1–5]

Synthesis of cubic Na_3PS_4 with high ionic conductivity (0.2 mS cm^{-1}) ignited interest in Na-based multinary chalcogenides.[6] Since then, extensive research has led to the development of a variety of ternary and quaternary compounds such as Na_3PnCh_4 (Pn = P, Sb, As, Ch = S, Se),[7–13] $Na_{11}Sn_2PnCh_{12}$,[14–16] $Na_{3-x}Pn_{1-x}W_xS_4$,[17] *etc.* Quaternary chalcogenides are typically formed through cation/anion doping of parent ternary compounds. The first reports of experimental and theoretical investigation of quaternary compounds in the Na–Sn–P–S system were inspired by highly conductive Li quaternary with $Li_{10}MP_2S_{12}$ (M = Si, Ge, Sn) composition.[18,19] These efforts resulted in the synthesis of $Na_{11}Sn_2PS_{12}$ (NSnPS), a slightly different stoichiometry than the original assumption, as the phase pure product of the Na–Sn–P–S system by different groups.[14,15] NSnPS possessed a newly explored tetragonal phase with $I4_1/acd$ space group and achieved high ionic conductivity (1.4–3.7 mS cm^{-2}) owing to the presence of vacancies in the crystal structure and three-dimensional network of Na^+ migration pathways.

Similar to ternary Na_3PS_4, the substitution of the phosphorous central atom with other pnictogens was attempted to address the air and moisture sensitivity of NSnPS according to the "hard and soft acid–base" (HSAB) theory. Using "softer" Sb resulted in an isostructural $Na_{11}Sn_2SbS_{12}$ (NSnSbS) with different sodium site occupations and vacancy, resulting in a slightly lower ionic conductivity (0.56 mS cm^{-2}). The difference in conductivity is attributed to changes in local bonding (P–S *vs.* Sb–S) and the lower electronegativity of Sb which leads to stronger Na–S coulombic attractions in the Sb quaternary.[20] In related work, Heo *et al.*[21] also reported $Na_{4-x}Sn_{1-x}Sb_xS_4$ ($0.02 \leq x \leq 0.33$) electrolytes derived through systematic doping of Na_4SnS_4 with Sb atoms. Moreover, the substitution of S atoms with Se was designed to improve the transport

Chemical and Biological Engineering, Colorado School of Mines, Golden, Colorado 80401, USA. E-mail: cwolden@mines.edu

† Electronic supplementary information (ESI) available. See DOI: https://doi.org/10.1039/d5ma00270b

© 2025 The Author(s). Published by the Royal Society of Chemistry

Open Access Article. Published on 02 July 2025. Downloaded on 5/21/2026 10:57:09 PM. This article is licensed under a Creative Commons Attribution-NonCommercial 3.0 Unported Licence.

properties of quaternary chalcogenides through lattice softening resulting in $Na_{11.1}Sn_{2.1}PSe_{12}$ composition.[22] However, structure-transport studies of $Na_{11}Sn_2SbS_{12-x}Se_x$ (x = 1, 6, and 12), solid-solution showed that the ionic conductivity decreases as the Se content is increased due to the change in the prefactor of the Arrhenius equation.[3]

In the majority of studies to date the quaternary chalcogenides were synthesized through high-temperature reactions between solid precursors in quartz ampoules, which is energy and time-intensive, and not amenable for industrial scale-up. This has prompted the development of liquid-based approaches which mitigate mass transfer limitations and enhance contact between reacting phases. In addition, the size and morphology of SSEs can be tuned by controlling liquid phase parameters such as solvent type, reagents chemistry, and reaction temperature. Hence, the choice of solvent becomes pertinent since aspects such as solubility and stability of reactants in the solvent and possible solvent complexes formation need to be considered.[23,24]

The liquid-phase reaction of chalcogenide SSEs can be divided into two categories: ''suspension'' and ''solution''. In the ''suspension'' approach, binary/elemental precursors are dispersed in organic solvents that facilitate the desired reaction by forming soluble reactive complexes. Following the reaction, the SSE precursor is isolated, and post-synthetic processing like annealing is typically required to induce crystallization or phase transformation. In contrast, the ''solution'' approach is built on the full dissolution of precursors and simultaneous formation of SSEs in polar protic solvents (*i.e.* water, EtOH) or amine–thiol co-solvents. The latter provides a homogenous solution that is useful in composite cathode processing. Also, crystallization obtained at low temperatures eliminates the need for further heat treatment.[25,26]

In this context, Yoon group attempted to extend their aqueous synthesis route of Na_3SbS_4 to $Na_{3.75}Sn_{0.75}Sb_{0.25}S_4$ (or $Na_{11.25}Sn_{2.25}Sb_{0.75}S_{12}$). As the stoichiometry is slightly different than the more stable 11-1-2-12 phase, a major phase of Na_3SbS_4 was yielded at 200 °C while a higher annealing temperature was required to induce the quaternary phase.[27] Hartmann and coworkers also explored the Sb doping in the Na_4SnS_4 compound through co-decomposition of the hydrated phase of Na_4SnS_4 and Na_3SbS_4 at 170 °C. Both $Na_4SnS_4{\cdot}14H_2O$ and $Na_3SbS_4{\cdot}9H_2O$ were crystallized from aqueous solutions of respective precursors.[28] In the case of $Na_{11}Sn_2PS_{12}$, Weng *et al.* reported the first liquid-phase synthesis by utilizing 1,2-dimethoxyethane (DME) that achieved 0.173 mS cm^{-1} conductivity. Though the samples sintered at high temperatures (>400 °C) showed the formation of tetragonal $Na_{11}Sn_2PS_{12}$, the as-recovered powder from the liquid phase reaction still contained a significant quantity of unreacted raw materials (*i.e.*, Na_2S and SnS_2) after a long reaction time. This observance along with the formation of unknown phases in the sintered sample indicates that the quaternary formation mainly occurred through sintering rather than liquid phase reaction.[29] In another pioneering study, the Yoon group extended the use of alkahest solvents (amine–thiol mixture) to a series of Li and Na SSEs including NSnPS using ethylenediamine (EDA) and 1,2-ethanedithiol (EDT) co-solvents. The as-synthesized NSnPS contained significant carbonaceous products upon high-temperature annealing due to the high boiling point of dithiols. Consequently, the obtained NSnPS had higher electronic conductivity than ionic conductivity.[25] Even though this approach was shown to be useful in producing composite cathodes, it is deemed unsuitable for the synthesis of pure NSnPS. The number of reports on the solution synthesis of quaternary chalcogenides is very limited and selenide quaternaries, in particular, have not yet been synthesized in the liquid phase. In addition, there is a lack of understanding about the underlying mechanism of these approaches. This inspired us to investigate the impacts of the various liquid-phase synthesis routes for a series of quaternary chalcogenides.

In this work, we first demonstrate the synthesis of phase pure $SnCh_2$ (Ch = S, Se) *via* a simple metathesis reaction between hydrated tin chloride and sodium chalcogenide solutions. The resulting $SnCh_2$ is then used as a precursor in the synthesis of $Na_{11}Sn_2PnCh_{12}$ (Pn = P, Sb, Ch = S, Se) electrolytes through liquid-phase reactions. We compare the efficacy of ''suspension'' and ''solution'' routes using aprotic, protic, and alkahest solvents in the context of these compounds. For each material, we outline the design principles and examine how key parameters such as reagent choice, solvent chemistry, and thermal post-treatment influence the formation mechanism, using a series of complementary characterization techniques such as XRD, FTIR, and Raman spectroscopy. Finally, the transport properties and electrochemical stability are probed through electrochemical impedance spectroscopy, DC polarization, and linear sweep voltammetry. Our findings identify $Na_{11}Sn_2SbS_{12}$ as the fastest ionic conductor and most stable quaternary composition for use in sodium all-solid-state batteries. This study demonstrates that Na-based quaternary chalcogenides can be designed and produced systematically through solvent-assisted approaches, further advancing the scalable production of solid-state electrolytes for Na ASSBs.

Experimental methods

Materials

Anhydrous Na_2S and highly pure Sb_2Ch_3 (Ch = S, Se) were produced according to previously reported works.[11,30,31] Phosphorus pentasulfide (P_2S_5, 99%, Sigma Aldrich), and elemental sulfur (S, Sigma Aldrich, 99.998% trace metal basis), sodium borohydride ($NaBH_4$, >98%, Sigma-Aldrich), selenium (Se, 99.99%, UMC), sodium (Na, Sigma-Aldrich), tin powder (Sn, Alfa Aesar, −325 mesh, 99.8%), tin(IV) chloride pentahydrate ($SnCl_4{\cdot}5H_2O$, 98+%, extra pure, Thermo Scientific Chemicals), sodium carbonate (Na_2CO_3, Alfa-Aesar, anhydrous ACS, 99.5% min), manganese(III) oxide (Mn_2O_3, Strem, 99%), iron(III) oxide (Fe_2O_3, Sigma Aldrich, 99%), acetonitrile (ACN, anhydrous, 99.8+%, Thermo Scientific Chemicals), ethanol (EtOH, Sigma-Aldrich, anhydrous, ≥99.5%), 1,2-ethylenediamine (EDA, Alfa Aesar, 99%), 1-propanethiol (PT, Thermo Scientific Chemicals,

© 2025 The Author(s). Published by the Royal Society of Chemistry

Open Access Article. Published on 02 July 2025. Downloaded on 5/21/2026 10:57:09 PM. This article is licensed under a Creative Commons Attribution-NonCommercial 3.0 Unported Licence.

98%), and UHP grade argon (Ar, 99.999%, General Air) were used as received without purification. Se pellets were further ground using a mortar and pestle to reduce particle size. All procedures were conducted in an Ar-filled glovebox (<5 ppm of H_2O) except otherwise stated.

Synthesis

Sb_2Ch_3 and Na_3SbCh_4 (Ch = Se, Se) were prepared as described in the literature.[11,31]

SnS_2. ~1.1 g batches of SnS_2 were produced as follows: $SnCl_4{\cdot}5H_2O$ (2105 mg, 6 mmol) were dissolved in 20 ml H_2O. Next, Na_2S (937.2 mg, 12 mmol) powder was slowly added to the tin solution. The metathesis reaction was instantaneous, and the solution turned orange. After stirring overnight, the solution was decanted and washed with excess H_2O multiple times to remove the NaCl byproduct. Extra grinding and washing steps were necessary to remove the remaining NaCl. The precipitate was dried under vacuum overnight and further annealed at 300 °C. Extra grinding and washing steps were necessary to remove the remaining NaCl (yield = 78.3%).

$SnSe_2$. First, the $NaBH_4$ solution was prepared by adding 529.1 mg (13.97 mmol) of $NaBH_4$ in 20 ml ethanol and stirring for 1 h to fully dissolve. Next, $NaBH_4$ solution was added dropwise to 920.3 mg (11.66 mmol) of Se in a three-neck flask that could facilitate the release of hydrogen gas. After stirring for 2 h at RT, a clear solution of NaHSe was formed. 20% excess $NaBH_4$ was used to ensure the full reduction of Se powder. In another container, 2043.2 mg (85.83 mmol) of $SnCl_4{\cdot}5H_2O$ was dissolved in 10 ml EtOH. Then, the tin solution was slowly added to the NaHSe solution and stirred overnight to ensure reaction completion. The solution was centrifuged and washed with excess water and EtOH consecutively and dried at RT for 12 h in vacuum (yield = 76.4%). The recovered powder was annealed under Ar flow at 300 °C in a horizontal tube furnace with a heating rate of 5 °C min^{-1} to remove the residual solvents and form crystalline $SnSe_2$.

$Na_{11}Sn_2PS_{12}$. 237 mg (3.04 mmol) Na_2S, 152 mg (1.10 mmol) SnS_2, and 61 mg (0.28 mmol) P_2S_5 were ground with a mortar and pestle. The mixture was dispersed in 10 ml of ACN and stirred at 50 °C for 2 days. The precipitate was recovered by multiple centrifugations and washing with excess ACN followed by vacuum drying at RT. The powder was pelletized and annealed under dynamic vacuum at various temperatures for 1 h with a fast heating rate (40 °C min^{-1}). A similar reaction was performed in EDA-PT mixture for 1 day at RT. In this case, the quaternary was recovered by discarding the undissolved precipitate and drying the supernatant at 150 °C under Ar flow in a tube furnace (yield = 90–94%).

$Na_{11}Sn_2SbS_{12}$. This reaction was conducted in EtOH, H_2O, and EDA-PT solvents. In this process, Na_2S (5% excess), S, as-synthesized SnS_2, and Sb_2S_3 were added to a 20 ml glass container, and respective solvents were added to the mixture. The H_2O and EDA-PT reactions were carried out at RT for 1 day while the ethanolic solution was heated at 50 °C for 2 days to ensure completion. In the case of EtOH, the solution was decanted and washed with excess EtOH multiple times, and the precipitate was recovered at RT under vacuum. In the case of H_2O, the solution was dried as-is at 150 °C under Ar flow in a horizontal tube furnace. The collected powder was dispersed in EtOH and washed multiple times with excess EtOH to recover the quaternary sulfide. A similar recovery procedure to the NSnPS (EDA-PT) sample was carried out to obtain NSnSbS (EDA-PT). Na_4SnS_4 was obtained by reacting 525.9 mg (1.5 mmol) of $SnCl_4{\cdot}5H_2O$ and 468.3 mg (6 mmol) of Na_2S in 5 ml H_2O. The solution was stirred for one day at 70 °C. To precipitate the Na_4SnS_4 crystals, 20 ml of MeOH was added to the aqueous solution and stored in the fridge at 4 °C for 2 days. The formed crystals were washed with excess MeOH and dried at 180 °C for 1 h under Ar flow (yield = 96.3%).

$Na_{11}Sn_2SbSe_{12}$

Aqueous reaction. First, NaHSe aqueous solution was prepared as follows: 454.2 mg (12 mmol) of $NaBH_4$ in 5 ml of water was slowly added to 395 mg (5 mmol) of Se at RT to prepare the aqueous NaHSe in a 25 ml flask. 20% excess $NaBH_4$ was used to ensure the full reduction of Se powder. After 1 h of reaction, the solution was cooled down to 4 °C and centrifuged to collect and discard the precipitate. Next, 364 mg (0.81 mmol) of Sb_2Se_3, 181.9 mg (4.55 mmol) of NaOH, 457.5 mg (1.65 mmol) of $SnSe_2$, and 65.3 mg (0.83 mmol) of Se were added to the NaHS solution. The solution was stirred at RT for two days. To collect the selenide precipitate, 8 ml of acetone was added to the solution and cooled at 4 °C for 1 day. After centrifugation and excess washing with acetone, the precipitate was dried overnight under vacuum at RT (yield = 42.6%) to obtain NSnSbSe powder. 2× NaOH was used to ensure a complete reaction.

Ethanolic reaction. Ethanolic NaHSe was prepared by first dissolving 124.8 mg (3.30 mmol) of $NaBH_4$ in 10 ml of EtOH and slowly adding to 217.1 mg (2.75 mmol) of Se powder in a 25 ml flask. Next, 276.6 mg (1 mmol) of $SnSe_2$, 120.1 mg (0.25 mmol) of Sb_2Se_3, 220 mg (5.5 mmol) of NaOH, and 39.5 mg (0.5 mmol) of Se were added to the ethanolic NaHSe. The solution was stirred at 50 °C for two days, decanted, and washed with EtOH twice. The precipitate was dried overnight under vacuum at RT (yield = 48.1%).

EDA-PT reaction. 109.2 mg (0.227 mmol) of Sb_2Se_3, 251.5 mg (0.91 mmol) of $SnSe_2$, 233.3 mg (2.99 mmol) of Se, and 115 mg (5 mmol) of Na were dissolved and reacted in 10 ml of EDA-PT (4-1) at RT inside the glovebox. After one day, the EDA-ET solution was centrifuged, and the collected supernatant was dried at 150 °C for 2 h under Ar flow in a tube furnace (yield = 73.3%). Recovered NSnSbSe was pelletized and further heat-treated at various temperatures for 1 h under vacuum in a custom-built quartz tube. Na_4SnSe_4 was obtained by reacting 276.6 mg (1 mmol) of $SnSe_2$, 157.9 mg (2 mmol) of Se, and 92 mg (4 mmol) of Na in 5 ml of EDA-PT (4-1) at RT. A similar recovery procedure was employed to obtain powder Na_4SnSe_4 (yield = 77.3%).

Na–Sn alloy. Na–Sn anodes are prepared by milling the stoichiometric amounts of finely cut Na and Sn powder (total mass of ~2 g) in a planetary mill (Across International, PQN2)

Open Access Article. Published on 02 July 2025. Downloaded on 5/21/2026 10:57:09 PM. This article is licensed under a Creative Commons Attribution-NonCommercial 3.0 Unported Licence.

at 510 rpm for 20 h. The milling cycles consisted of 15 min of milling and 15 min of rest (yield = 65%).

Materials characterization

Thermogravimetric analysis and differential scanning calorimetry (TGA/DSC) were performed on a TA Instruments SDT-Q600 model. For a typical run, 10 mg of sample was loaded into a pre-cleaned alumina pan and heated under flowing Ar from RT to 600 °C at 10 °C min^{-1} rate and then cooled down naturally. X-ray diffraction (XRD) was performed with a Philips X'Pert X-ray diffractometer with Cu Kα radiation (λ = 0.15405 nm) between 10 and 60° at a scan rate of 5° min^{-1}. Samples were prepared on a glass slide with a protective tape covering the material to prevent undesired reactions with ambient air. XRD background subtraction was performed using HighScore software. Raman spectroscopy was conducted with a WiTec alpha 300 M confocal microscope/Raman spectrometer employing a 100 mW 532 nm laser. Samples were mounted on a glass slide and sealed under a 0.1 mm quartz cover slip. The laser was focused through the coverslip onto the sample using a 20× objective, and spectra were collected using a CCD detector (Andor Technologies) at −60 °C. HighScore software was used to subtract the Raman background.

Field emission scanning electron microscopy (FESEM) images were collected on a JEOL JSM-7000F FESEM instrument equipped with energy-dispersive X-ray spectroscopy (EDX) for compositional analysis. To prepare the samples for SEM and EDX measurements, powder samples were immobilized onto an aluminum stub using double-sided carbon tape. An accelerating voltage of 5 kV was used for the SEM image, while a higher voltage of 15–20 V was employed for EDX spectra collection. All sample preparation was done in an Ar glovebox.

Electrochemical characterization

Conductivity measurements. Pellets of quaternary SSE were prepared for conductivity measurement *via* conventional uniaxial pressing. For this purpose, 150–250 mg of the electrolyte was loaded into a 12 mm PEEK split cell with stainless steel plungers under a uniaxial fabrication pressure of 270 MPa and held for 5 min. Pellets were typically 0.9–1.1 mm thick (~75–90% densification). The SSE pellets were contacted using stainless steel plungers as ion-blocking electrodes for electrochemical characterization. The pressure was released for 1 min, then increased again to 75 MPa. A Gamry Interface 1000E potentiostat was used to perform electrochemical impedance spectroscopy (EIS) measurements across a frequency range of 1 Hz to 1 MHz with a 10 mV perturbation. Temperature-dependent EIS testing was performed by heating the split cell apparatus with an electrical heating element and allowing it to stabilize at the target temperature for 1.5 h. DC polarization measurements were performed by applying multiple-step potentials to the sample (0.1, 0.2, 0.3, 0.4, and 0.5) and recording the transient current. The steady-state current was recorded after 2 h at each step potential, and the electrical conductivity was calculated using Ohm's law.

Symmetric cell cycling. Sodium plating/stripping cycling was performed in symmetrical Na–Sn|SSE|Na–Sn cells with a current density of 0.02 mA cm^{-2} at 60 °C. To assemble the symmetric cell, 150 mg of SSE was cold pressed in a PEEK split cell at 270 MPa. Then, 50 mg of Na–Sn anode powders were dispersed on both sides of the pellet and pressed together at 340 MPa for 5 min. The finished cell was clamped in an in-house built pressure jig fixated at 50 MPa. Galvanostatic charging and discharging (30 min per step) were performed after aging the cell at 60 °C for 2 h by a battery tester (MTI Corporation, BST8-MA).

Linear sweep voltammetry (LSV). LSV was performed on two Na–Sn|SSE|SS-SSE cells at RT using Gamry potentiostat. To fabricate the cells, stainless steel (SS) powder and SSE were hand-ground with a 21 : 9 ratio in a mortar to form the working electrode. The separator layer was formed by pressing 100 mg of the electrolyte at 150 MPa (5 min) in a 12 mm PEEK cell. Next, 20 mg of the working electrode was dispersed on the separator carefully and pressed at 275 MPa for 5 min. Lastly, the reference/counter electrode was formed by adding 60 mg Na–Sn on the other side of the separator layer and pressing the system at 275 MPa for 5 min. The stacking pressure of 50 MPa was applied during measurements. The cathodic and anodic scans were measured on the ranges open circuit voltage (OCV) −5 V and OCV −0 V at a scanning rate of 0.1 mV s^{-1}, respectively.

Results and discussion

$SnCh_2$ metathesis

One key challenge in developing Na-based solid-state electrolytes (SSEs) is the limited accessibility of their binary precursors. Binary chalcogenides, such as Na_2Ch, Sb_2Ch_3, and $SnCh_2$, are essential components and significant cost drivers for various components of Na all-solid-state batteries (ASSBs). However, their synthesis is typically expensive and primarily available for research purposes.[11,31,32] $SnCh_2$ compounds, in particular, feature layered structures held together by van der Waals forces, which impart excellent optical and electronic properties. Wet chemical methods, including solvothermal[33–36] and colloidal approaches,[37–40] have been reported for synthesizing $SnCh_2$. Solvothermal synthesis typically requires autoclaves capable of withstanding high pressure and temperature, while the colloidal method uses high boiling point solvents at elevated temperatures. Although these techniques yield size-controlled and highly pure tin chalcogenides, their complex reaction mechanisms, specialized equipment, and toxic precursors hinder their viability for large-scale production.

In this context, we employed simple metathesis reactions in polar solvents (H_2O and EtOH) followed by mild heat treatment to produce the $SnCh_2$ required for quaternary synthesis. Metathesis involves the exchange of counterions between two chemical species, often resulting in the precipitation of one product, which offers favorable energetics and facile separation. The salts used in this process are generally low-cost and

© 2025 The Author(s). Published by the Royal Society of Chemistry

Open Access Article. Published on 02 July 2025. Downloaded on 5/21/2026 10:57:09 PM. This article is licensed under a Creative Commons Attribution-NonCommercial 3.0 Unported Licence.

readily available.[41,42] The reactions used for the synthesis of SnS_2 and $SnSe_2$ in this work are outlined in eqn (1) and (2), respectively.

$$2Na_2S_{(aq)} + SnCl_4{\cdot}5H_2O_{(aq)} \rightarrow SnS_{2(s)} + 4NaCl_{(aq)} + 5H_2O_{(l)} \quad (1)$$

$$2NaHSe_{(sol)} + SnCl_4{\cdot}5H_2O_{(sol)} \rightarrow SnSe_{2(s)} + 2NaCl_{(sol)} + 2HCl_{(sol)} + 5H_2O_{(l)} \quad (2)$$

Fig. 1a shows the XRD patterns of $SnCh_2$ compounds obtained from their respective reactions. For SnS_2, the reaction was performed in H_2O, and the resulting precipitate was thoroughly washed with excess water to remove the NaCl by-product. The sulfide was then recovered by vacuum drying at room temperature. Since the reduction of Se in water tends to produce persistent borax impurities, the $SnSe_2$ reaction was instead conducted in ethanol, following a similar recovery process as for SnS_2.[31,43] The amorphous $SnCh_2$ powders obtained at room temperature were further heat-treated to enhance their crystallinity (Fig. S1 and S2, ESI†). Thermogravimetric analysis (TGA) revealed that a temperature of 300 °C was necessary to completely remove the solvate complexes in SnS_2 (Fig. S1a, ESI†).

The annealed SnS_2 exhibited a cubic structure (space group *Fd*3*m*), with the presence of pure cubic NaCl confirmed in the supernatant (Fig. S1b, ESI†). Additionally, the Raman spectra of the annealed SnS_2 showed the characteristic SnS_2 peak at 313 cm^{-1}, verifying its phase purity (Fig. 1b).[44] The annealed $SnSe_2$ sample displayed a CdI2-type hexagonal layered structure with *P*3*m*1 symmetry. Raman analysis also confirmed the presence of $SnSe_2$, with peaks at 187 cm^{-1} and 117 cm^{-1} corresponding to the A_{1g} and E_g modes of $SnSe_2$, respectively.[35,40] In addition to $SnCh_2$ compounds developed here, other binaries precursors, such as Sb_2Ch_3, were synthesized using the metathesis method as described in detail in our previous works.[11,31]

Synthesis of $Na_{11}Sn_2PS_{12}$

The quaternary reaction to synthesize NSnPS was performed with Na_2S, SnS_2, and P_2S_5 as precursors according to the following stoichiometry (eqn (3)):

$$11Na_2S + 4SnS_2 + P_2S_5 \rightarrow 2Na_{11}Sn_2PS_{12} \quad (3)$$

The choice of solvents for chalcogenide synthesis depends on factors like dielectric constant, polarity, and molecular composition, which influence the solubility and stability of reagents in the solvent. The dielectric constant (ε_r) reflects the solvent's ability to dissolve precursors. Polar solvents, such as water (H_2O) and ethanol (EtOH), have high dielectric constants due to hydrogen bonding. However, they are unsuitable for P-containing chalcogenides like Na_3PS_4 and $Na_{11}Sn_2PS_{12}$, as they have been shown to decompose P_2S_5 and PS_4^{3-} moieties (Table S1, ESI†).[45] In contrast, aprotic solvents such as DME, diethyl ether (DEE), ethyl propionate (EP), ethyl acetate (EA), and ACN have been used in the Na_2S–P_2S_5 system.[46–49] These solvents are capable of forming reactive complexes without hydrolyzing the P_2S_5 precursor. ACN, in particular, offers both a high dielectric constant and easy solvent removal due to its low boiling point. Additionally, reagents like P_2S_5 and SnS_2 are shown to be stable and well-dispersed in non-polar ACN, promoting uniform mixing.

Building on these findings, we selected ACN as the reaction medium for the "suspension" synthesis of $Na_{11}Sn_2PS_{12}$. In this experiment, stoichiometric amounts of Na_2S, P_2S_5, and freshly prepared SnS_2 were dispersed in ACN and reacted at 50 °C for 2 days. The resulting precipitate was recovered and washed with excess ACN before drying at room temperature under vacuum. The obtained powder was then heat-treated at various temperatures under vacuum to promote the solid-state reaction and enhance crystallinity. XRD and Raman analyses were conducted to assess the phase purity of the synthesized NSnPS materials and to investigate the formation mechanisms of the ternary and quaternary phases (Fig. 2a and b). The XRD pattern of the sample recovered at room temperature shows the

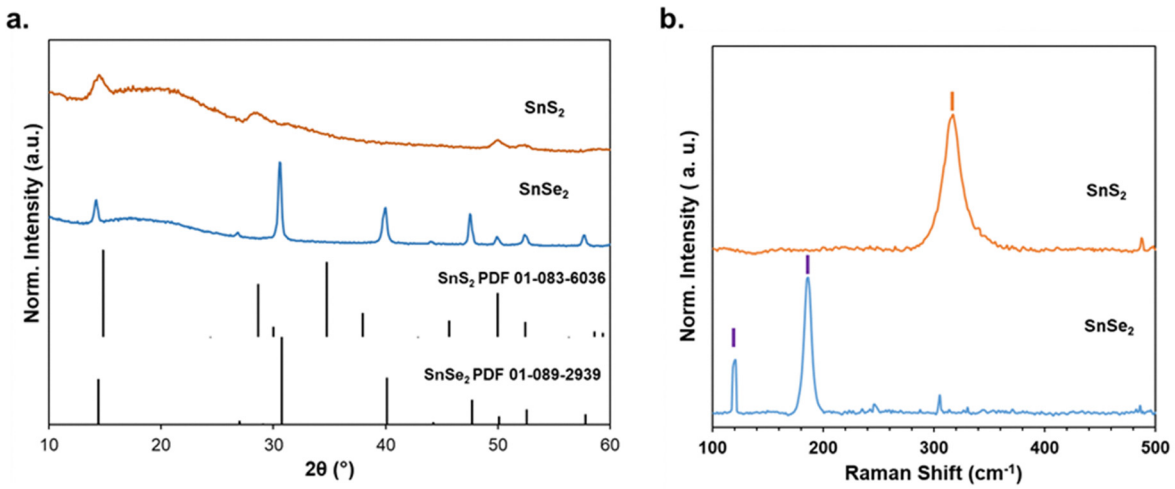

Fig. 1 (a) XRD and (b) Raman spectra of $SnCh_2$ (Ch = S, Se) recovered from metathesis reactions after annealing at 300 °C.

Open Access Article. Published on 02 July 2025. Downloaded on 5/21/2026 10:57:09 PM.
This article is licensed under a Creative Commons Attribution-NonCommercial 3.0 Unported Licence.

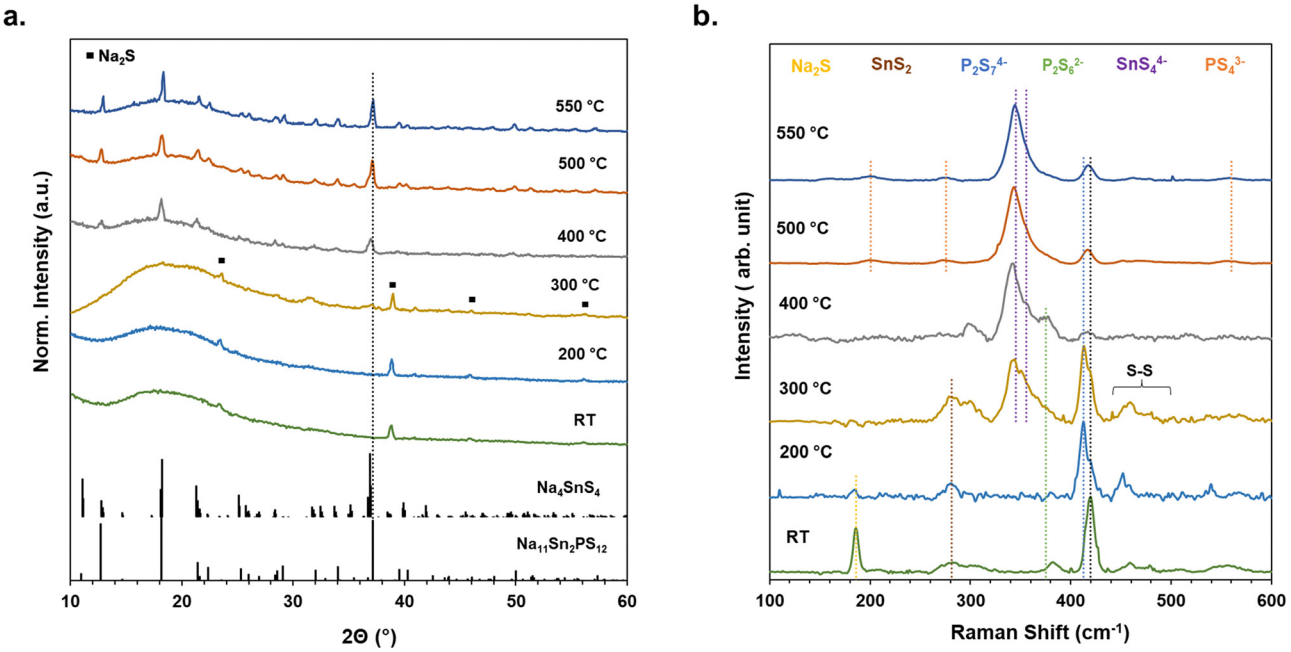

Fig. 2 (a) XRD, and (b) Raman spectra of NSnPS recovered from ACN and heat-treated at different temperatures.

presence of unreacted Na_2S; however, the Raman and FTIR spectra (Fig. S3, ESI†) indicate the formation of PS_4^{3-}, $P_2S_7^{4-}$, and $P_2S_6^{4-}$ polyanions along with small traces of Na_2S and SnS_2, S–S bonds. The deconvoluted Raman spectra are presented in Fig. S4 (ESI†). Annealing at 200 °C did not cause any significant change in the XRD pattern of the NSnPS sample, but the Raman peaks attributed to P–S bonds indicated a potential shift in the intensity of $[PS_4^{4-}]$ and $[P_2S_7^{4-}]$ polyhedra, suggesting a possible transition from amorphous Na_3PS_4 to $Na_4P_2S_7$.[50–54] This reaction, which involves the release of Na_2S, can be represented as follows:

$$2Na_3PS_4 \rightarrow Na_4P_2S_7 + Na_2S \quad (4)$$

At 300 °C, a major peak at 342 cm^{-1}, accompanied by a strong shoulder at approximately 356 cm^{-1}, indicates the formation of $Sn_2S_6^{4-}/SnS_4^{4-}$ anions. However, there is no crystallographic evidence of Na_4SnS_6 formation in the XRD pattern.[55] Since Na_4SnS_4 and $Na_4Sn_2S_6$ exhibit very similar Raman vibration modes, it is challenging to definitively rule out the formation of either or a potential mixed polyanion compound without additional characterization techniques such as NMR.[55,56] In contrast, Duchardt *et al.*[57] demonstrated that the formation of NSnPS is accompanied by a blue shift to higher wavenumbers in the symmetric stretching vibration of Sn–S (345 cm^{-1}) and P–S (417 cm^{-1}) bonds compared to their original position in the corresponding Na_4SnS_4 (340 cm^{-1}) and Na_3PS_4 (412 cm^{-1}) compounds. The presence of a doublet peak in the 342–356 cm^{-1} range may indicate the onset of NSnPS formation. Additionally, the peaks at 280.7 and 299.7 cm^{-1} could be assigned SnS_2 and Sn–S–Sn bonds, respectively.[55] Although Na_2S remains the major crystalline phase, broad peaks associated with Na_4SnS_4/NSnPS appear in the XRD pattern, further confirming the Raman observations. Therefore, we can speculate that a minimum temperature of 300 °C is necessary for the onset of quaternary phase formation.

Further increasing the temperature stabilizes the quaternary phase, with minor precipitation of the Na_4SnS_4 phase. Raman analysis also confirms the consumption of $[PS_4^{3-}]$ and $[P_2S_7^{4-}]$ polyanions, likely through a solid-state reaction with available Na_4SnS_4 and Na_2S to generate the quaternary phase (eqn (5) and (6)). At this stage, all unreacted SnS_2 is converted into ternary and quaternary phases, indicating the consumption of all binary precursors. The peak at 375 cm^{-1} could be attributed to the characteristic P–P stretching mode of $[P_2S_6^{4-}]$ polyanion, which is likely generated as a side product of high-temperature annealing through the release of S atoms from $Na_4P_2S_7$.[51]

$$Na_2S + SnS_2 \rightarrow Na_4SnS_4 \quad (5)$$

$$Na_3PS_4 + \frac{1}{2}Na_4P_2S_7 + \frac{1}{2}Na_2S + 4Na_4SnS_4 \rightarrow 2Na_{11}Sn_2PS_{12} \quad (6)$$

Higher temperatures of 500 and 550 °C further reduce the concentration of Na_4SnS_4, indicating its incorporation into the quaternary phase. As the concentration of Na_4SnS_4 decreases, the Sn–S vibrations of NSnPS shift toward higher wavenumbers. Nevertheless, the ternary phase remains present, as Rietveld refinement for the 550 °C sample indicates a 4.7 wt% Na_4SnS_4 (Fig. S5, ESI†). The as-synthesized NSnPS exhibits a tetragonal phase (space group $I4_1/acd$, PDF 04-025-2554) with lattice parameters of $a = b = 13.6472\ 1736$ Å, $c = 27.3634$ Å, and $V = 5096.52$ $Å^3$, which aligns closely with previous reports of NSnPS synthesized *via* solid-state reactions.[14,15] The corresponding FTIR data also reveals small traces of P–O bonds, likely due to oxidation during sample handling (Fig. S4, ESI†).

© 2025 The Author(s). Published by the Royal Society of Chemistry

Open Access Article. Published on 02 July 2025. Downloaded on 5/21/2026 10:57:09 PM.
This article is licensed under a Creative Commons Attribution-NonCommercial 3.0 Unported Licence.

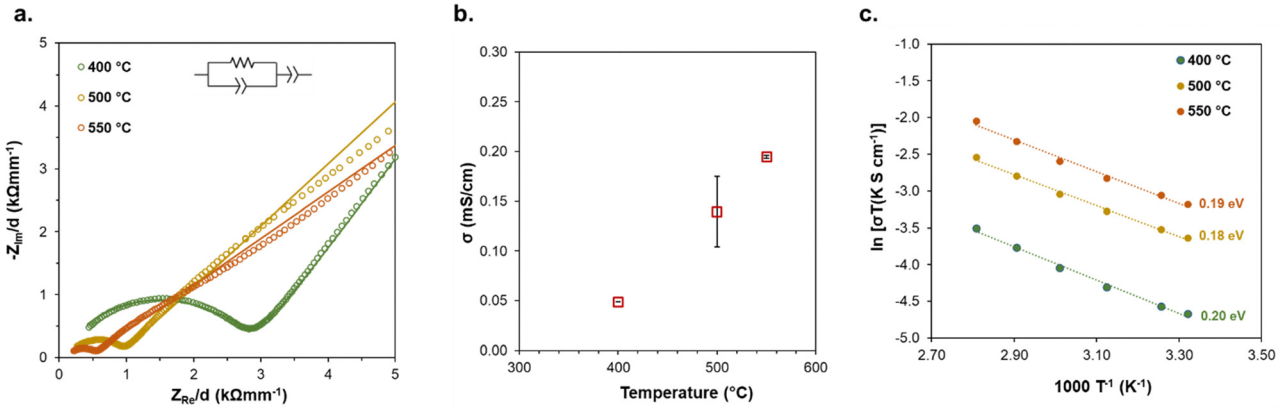

Fig. 3 (a) Nyquist plots, (b) corresponding ionic conductivity, and (c) Arrhenius plots of NSnPS synthesized in ACN as a function of annealing temperature.

The ionic transport properties of NSnPS recovered from ACN were investigated over a wide range of temperatures and frequencies using EIS. Fig. 3a shows the Nyquist plots of NSnPS heat-treated at different temperatures, while the extracted total conductivity values from equivalent circuit fitting are presented in Fig. 3b. The spectra were fitted to the equivalent circuit that consisted of a parallel combination of a resistor and constant phase element (CPE), which describes the suppressed semicircle, in series with another CPE that corresponds to electrode polarization (inset of Fig. 3a). Upon annealing from 300 °C to 550 °C, we observed an improvement in the ionic conductivity, correlating with the reduction in the concentration of Na_4SnS_4, highlighting the importance of phase purity on ionic transport in quaternary NSnPS. The highest ionic conductivity of 0.2 mS cm^{-1} was achieved at 550 °C, which is in good agreement with the other reports of NSnPS synthesized through liquid phase routes (Table 1).[25,29] Even though the obtained conductivity is not explicitly superior to the other studies due to the presence of a low-conductive Na_4SnS_4 phase, the detailed investigation into the solvent influence and identification of potential impurities in this system is highly valuable and could serve as a roadmap for the synthetic design of similar materials.

The kinetics of Na^+ transport were investigated through temperature-dependent EIS. Fig. 3c presents the Arrhenius plots for the corresponding annealed NSnPS, with activation energies extracted in the temperature range of 25–100 °C. The obtained activation energy values (0.18–0.20 eV) are slightly lower than those reported from other groups, potentially due to variations in experimental setups, off-stoichiometry, and the presence of impurity phases such as Na_4SnS_4 in the quaternary compounds (Table 1). The electronic conductivity of NSnPS compounds was measured using DC polarization in a symmetric cell configuration (Ti|SSE|Ti), similar to the EIS experiments. For the sample annealed at 550 °C, an electronic conductivity value of $\sigma_e = 5.7 \times 10^{-6}$ mS cm^{-2} was obtained which was on the same order of magnitude as NSnPS derived from DME solvent in the report by Weng and coworkers.[29]

We also explored the alkahest amine–thiol approach for the NSnPS reaction. For this, we selected a mixture of ethylenediamine (EDA) and propanethiol (PT) due to their combined lower boiling point compared to diamine–dithiol co-solvents. Lee

Table 1 Summary of quaternary synthesis parameters and performance reports in the literature

Quaternary	Synthesis method	Precursors	Heat-treatment (°C)	σ_{Na^+} (mS cm^{-1})	E_a (eV)	Electrochemical window *vs.* Na^+/Na (V)	Ref.
$Na_{11}Sn_2PS_{12}$	Solid-state (700 °C, 5 h)	Na_2S, P_2S_5, SnS_2	—	1.4	0.25	—	14
$Na_{11}Sn_2PS_{12}$	Solid-state (600 °C)	Na_3PS_4, Na_4SnS_4	—	3.7	0.39	—	15
$Na_{11}Sn_2PS_{12}$	Suspension (DME)	Na_2S, P_2S_5, SnS_2	460	0.17	0.33	0.3–3.2	29
$Na_{11}Sn_2SbS_{12}$	Solid-state (700 °C, 5 h)	Na_2S, Sb_2S_3, SnS_2, S	—	0.56	0.34	—	20
$Na_{4-x}Sn_{1-x}Sb_xS_{12}$ ($0.02 \leq x \leq 0.33$)	Solid-state (450–550 °C, 12 h)	Na_2S, Sb_2S_3, SnS_2, S	550	0.51 ($x = 0.25$)	0.39 ($x = 0.25$)	~0.4–4.5	21
$Na_{11.1}Sn_{2.1}PSe_{12}$	Solid-state (600 °C, 12 h)	Na_2Se, Sn, P, Se	600	1.7	0.30	—	22
$Na_{11}Sn_2PSe_{12}$	Solid-state (900 °C, 48 h)	Na_2Se, Sn, P, Se	900	2.15	0.28	1.22–2.65	58
$Na_{11}Sn_2PSe_{12}$	Milling (400 rpm, 15 h), annealing (600 °C)	Na, Sn, P, Se	550	0.13	—	—	59
$Na_{11}Sn_2SbSe_{12}$	Milling (33 h, 400 rpm) solid-state (750 °C, 5 h)	Na_2Se, Sb_2Se_3, $SnSe_2$, Se	750	0.15	0.39	—	3
$Na_{11}Sn_2PS_{12}$	Suspension (ACN)	Na_2S, P_2S_5, SnS_2	550	0.2	0.19	0.95–1.7 V	This
$Na_{11}Sn_2SbS_{12}$	Solution (H_2O)	Na_2S, Sb_2S_3, SnS_2, S	550	0.42	0.14	1.15–3.1 V	work
$Na_{11}Sn_2SbSe_{12}$	Solution (EDA-PT)	Na, Sb_2Se_3, $SnSe_2$, Se	550	0.07	0.22	0.85–2.0 V	

Open Access Article. Published on 02 July 2025. Downloaded on 5/21/2026 10:57:09 PM. This article is licensed under a Creative Commons Attribution-NonCommercial 3.0 Unported Licence.

et al.[25] previously demonstrated that P_2S_5 fully dissolves in EDA-ethanethiol (ET) solvents without any noticeable hydrolysis. Our attempt with EDA-PT yielded a compound with an XRD pattern similar to what was reported in their study. A closer examination of the XRD pattern, coupled with Raman analysis (Fig. S6, ESI†), indicated the formation of ternary Na_4SnS_4 with a tetragonal phase (space group $I4_1/acd$), rather than the expected $Na_{11}Sn_2PS_{12}$ in the diamine–monothiol solvents. Interestingly, Hartmann *et al.*[28] recently identified this new phase of Na_4SnS_4, which is isostructural to NSnPS and NSnSbS compounds, through controlled dehydration of $Na_4SnS_4{\cdot}14H_2O$ crystals.

Based on these observations, we can infer that the formation of $Na_{11}Sn_2PS_{12}$ in EDA-EDT as described by Yoon group,[25] but not in EDA-PT, is closely related to the specific nature of P_2S_5 dissolution and the thiolate species produced in these systems. A recent study on chalcogen dissolution in amine–thiol solutions found that the type of amine and thiol can significantly impact the reactive intermediates formed, which, in turn, influences subsequent reactions.[60] Further investigations are needed to elucidate the specific reaction pathway that facilitates phosphorus incorporation to form NSnPS in diamine–dithiol solvents. In conclusion, the suspension synthesis of NSnPS with ACN proves to be the optimal choice over the diamine–dithiol approach owing to its less complicated synthesis procedure, lower electronic conductivity, and use of benign and environment-friendly solvent. ACN offers a safer alternative compared to the relatively toxic amine–thiol cosolvents.

Synthesis of $Na_{11}Sn_2SbS_{12}$

$Na_{11}Sn_2SbS_{12}$ enhances the air stability relative to its isostructural analog, $Na_{11}Sn_2PS_{12}$. Sb-based and Sn-based chalcogenides such as Na_3SbCh_4 and Na_4SnCh_4 (Ch = S, Se) can be synthesized in polar solvents like H_2O, MeOH, and EtOH. For example, the aqueous solution synthesis of Na_4SnS_4 has been reported with $Na_2S{\cdot}9H_2O$, $SnCl_4$, or SnS_2 precursors.[61,62] We recently investigated different synthetic protocols for Na_3SbCh_4 compounds in EtOH and demonstrated that the formation of reactive Na chalcogenides is a critical step in producing highly pure Na_3SbCh_4.[11,31,43] In these compounds, the nucleophilic attack of the chalcogenide ions on the binary chalcogenides, such as Sb_2Ch_3, promotes the formation of $[SbCh_3]^{3-}$ anions, followed by the reduction of elemental chalcogen to produce $[SbCh_3]^{4-}$ polyhedral anions. We hypothesized that a similar chemistry would be feasible in the synthesis of $Na_{11}Sn_2SbS_{12}$, utilizing the formation of $[SbS_4]^{3-}$ and $[SnS_4]^{4-}$ polyanions. Accordingly, the following reaction scheme was attempted in H_2O and EtOH:

$$11Na_2S + Sb_2S_3 + 4SnS_2 + 2S \rightarrow 2Na_{11}Sn_2SbS_{12} \quad (7)$$

Sodium sulfide was prepared by dehydration and reduction of the low-cost technical grade hydrate ($Na_2S{\cdot}xH_2O$)[30] and the other binary sulfide precursors were procured *via* metathesis as discussed above. Since NSnSbS is soluble in H_2O, it is necessary to use an antisolvent, such as EtOH or acetone, to separate the quaternary compound. In this experiment, Na_2S (with a 10% excess), freshly prepared SnS_2, Sb_2S_3, and S were dispersed in H_2O and reacted at room temperature. The slight excess of Na_2S was intended to ensure complete reaction. To recover NSnSbS, the aqueous solution was dried at 150 °C under an inert argon atmosphere and washed with excess EtOH to remove unreacted precursors and soluble intermediates.

The reaction in EtOH was conducted with a similar stoichiometry. Initial attempts indicated slow kinetics for NSnSbS formation in the less polar EtOH; therefore, the solution was heated to 50 °C for an extended period (2 days) to ensure a complete reaction. Since NSnSbS is insoluble in EtOH, this approach facilitated its direct precipitation at room temperature. The sample recovered from EtOH was further dried at 150 °C to eliminate any remaining solvent and to ensure consistent heat treatment with the aqueous experiment. Additionally, we investigated the applicability of amine–thiol co-solvents for this stoichiometry. Pioneering work by the Butchery group has demonstrated the dissolution and redeposition of binary chalcogenides, such as Sb_2Ch_3 and SnS_2, in amine–thiol co-solvents.[63,64] Since all precursors are sufficiently soluble in the EDA-PT mixture, this reaction was performed at room temperature for 1 day, and the powder was recovered by discarding unreacted precipitate and drying the supernatant at 150 °C.

Fig. 4a shows the XRD patterns of compounds obtained from H_2O, EtOH, and EDA-PT solvents, with reference patterns for Na_4SnS_4 and Na_3SbS_4 included for comparison. Detailed synthesis protocols for Na_4SnS_4 and Na_3SbS_4 in aqueous solutions can be found in the Experimental section. The $Na_{11}SnSbS_{12}$ recovered from all solvents exhibits a tetragonal crystalline phase ($I4_1/acd$ space group) consistent with the reported structure for this compound.[20,21] The NSnSbS obtained from an aqueous solution is highly crystalline highlighting the effectiveness of highly polar solvents in promoting room-temperature crystallization of quaternary chalcogenides. In contrast, the powders recovered from EtOH and EDA-PT solvents exhibited lower crystallinity with small traces of Na_3SbS_4 detected. Since NSnSbS is isostructural with the Na_4SnS_4 recovered from the aqueous solution, XRD alone is inconclusive regarding the formation of NSnSbS.[28] Therefore, Raman spectroscopy was conducted to provide deeper insights into their molecular order and to assess the influence of Sb doping on the structure.

The corresponding Raman spectra are depicted in Fig. 4b. To accurately identify the existing vibrational modes, peak deconvolution was conducted for the Raman peaks of the samples recovered from H_2O, EtOH, and EDA-PT (see Fig. S7, ESI†). The NSnSbS obtained from the aqueous solution displays peaks at approximately 341 cm^{-1} and 363 cm^{-1}, which corresponds to the symmetric vibration (ν_s) of Sn–S and Sb–S, respectively. For the asymmetric stretching modes of the SbS_4 anions, expected peaks at ν_a = 385 cm^{-1} and 403 cm^{-1} were observed in the pure Na_3SbS_4 sample.[65] However, in the H_2O-recovered sample, these peaks merged into a broader peak at 399 cm^{-1}, indicating a change in the local structure due to the incorporation of Sn. Additionally, a strong peak at 372 cm^{-1} can be attributed to the $[SbS_4]$ polyhedra within the quaternary

© 2025 The Author(s). Published by the Royal Society of Chemistry

Open Access Article. Published on 02 July 2025. Downloaded on 5/21/2026 10:57:09 PM.
This article is licensed under a Creative Commons Attribution-NonCommercial 3.0 Unported Licence.

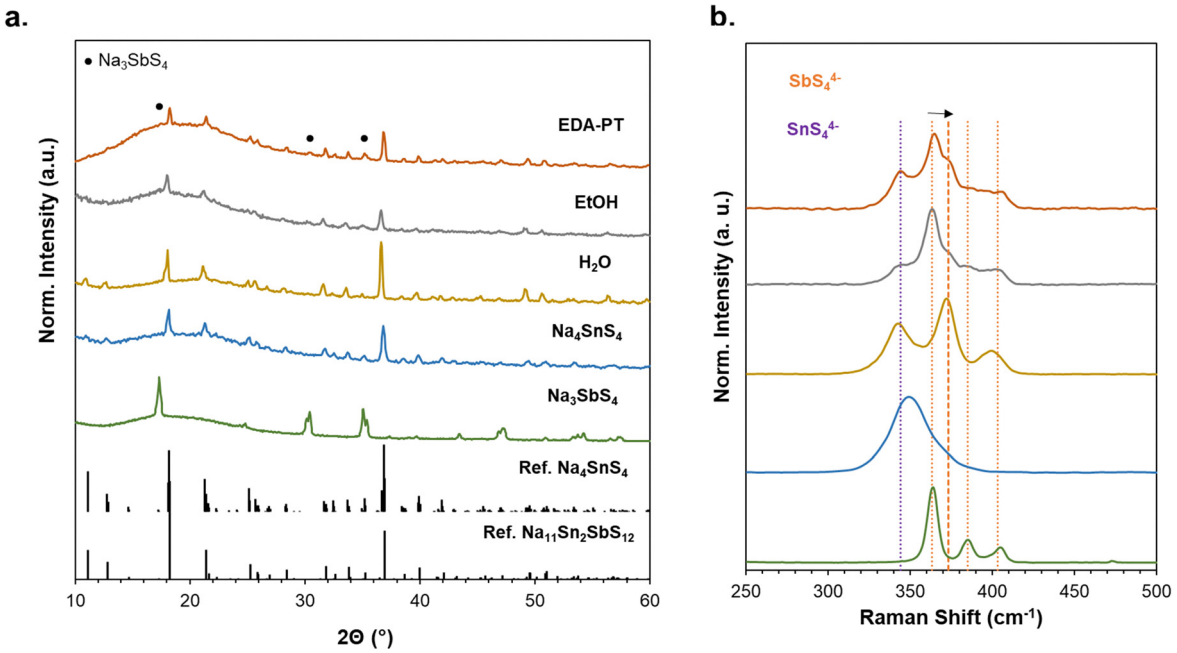

Fig. 4 (a) XRD, and (b) Raman of NSnSbS recovered from different solvent systems and dried at 150 °C.

lattice framework. The NSnSbS structure features two types of isolated SnS_4 (or SbS_4) tetrahedra, positioned on distinct Sn-only sites and an Sb mixed site.[20]

The XRD pattern of NSnSbS obtained from EtOH and EDA-PT shows a strong presence of pure Na_3SbS_4, which is further emphasized by the high-intensity Sb–S stretching mode at 363 cm^{-1} in the corresponding Raman spectra. The emergence of a peak at 372 cm^{-1} as a smaller shoulder supports the direct correlation between the [SbS_4] peak signature and the extent of Sb incorporation into the quaternary lattice. Similar to the findings for NSnPS, a blue shift in the Raman peaks of the SbS_4 and SnS_4 polyanions was observed, likely due to alterations in the local bonding environment compared to the constituent ternary Na_3SbS_4 and Na_4SnS_4.[56,65] The Raman analysis provides clear evidence for the generation of quaternary $Na_{11}Sn_2SbS_{12}$ compounds; however, higher-resolution X-ray or neutron diffraction studies are necessary to fully elucidate the local crystal structure of the formed quaternary.

To enhance the Na^+ transport properties, the NSnSbS powders were annealed at 550 °C under vacuum. Fig. S8 (ESI†) shows the XRD patterns of annealed NSnSbS samples. The aqueous-recovered sample shows no apparent secondary phases, while the ethanolic NSnSbS exhibits traces of $NaSbS_2$, likely formed from the decomposition of the Na_3SbS_4 phase at high temperatures. The sample recovered from EDA-PT indicates only traces of Na_3SbS_4. The ionic and electronic conductivities of the samples are summarized in Fig. 5a. As expected, the aqueous-recovered NSnSbS, having the highest crystallinity and phase purity, demonstrates a maximum conductivity of 0.42 mS cm^{-1} at room temperature – approximately four times higher than the other samples containing $NaSbS_2$ impurities. The electronic conductivity across all samples ranges from 3.8×10^{-7} to 3.1×10^{-6} mS cm^{-1}, rendering them suitable superionic conductors.

Fig. 5b displays the Arrhenius plots for the NSnSbS samples, indicating a low activation barrier for the aqueous-recovered NSnSbS, attributed to its high crystallinity and phase purity. Additionally, Fig. S9 (ESI†) provides the XRD and Raman spectra from the heat treatment studies conducted on NSnSbS recovered from aqueous solutions. The trend of ionic conductivity as a function of temperature (Fig. S9c, ESI†) illustrates nearly a twofold increase in the ionic conductivity of the quaternary phase as the annealing temperature rises to 550 °C. This enhancement is likely due to the complete incorporation of Sb into the quaternary lattice and the removal of solvated complexes. Overall, these findings highlight the potential of aqueous synthesis methods for developing Sn and Sb-based chalcogenide solid-state electrolytes.

Synthesis of $Na_{11}Sn_2SbSe_{12}$

Lastly, we focused on quaternary selenides with the composition $Na_{11}Sn_2PnSe_{12}$ (where Pn = P, Sb). The common precursors for this class typically include elemental Na, P, Se, or binary selenides such as Na_2Se, $SnSe_2$ and Sb_2Se_3. As for the Sb analog, we explored various activated Se precursors in polar solvents, since aprotic solvents are not suitable due to the insoluble nature of elemental Se. Our attempts to synthesize NSnSbSe using aqueous and ethanolic solutions of NaHSe, following the reaction scheme outlined in eqn (8), led to the formation of Na_3SbSe_4. However, there was no apparent doping of Sn into the lattice structure of the resultant compound, as evidenced by the data presented in Fig. S10 (ESI†).

$$11NaHSe_{(sol)} + Sb_2Se_{3(s)} + 4SnSe_{2(s)} + 3Se_{(s)} + 11NaOH_{(sol)} \rightarrow 2Na_{11}Sn_2SbSe_{12(s)} + 11H_2O_{(l)} \quad (8)$$

Open Access Article. Published on 02 July 2025. Downloaded on 5/21/2026 10:57:09 PM.
This article is licensed under a Creative Commons Attribution-NonCommercial 3.0 Unported Licence.

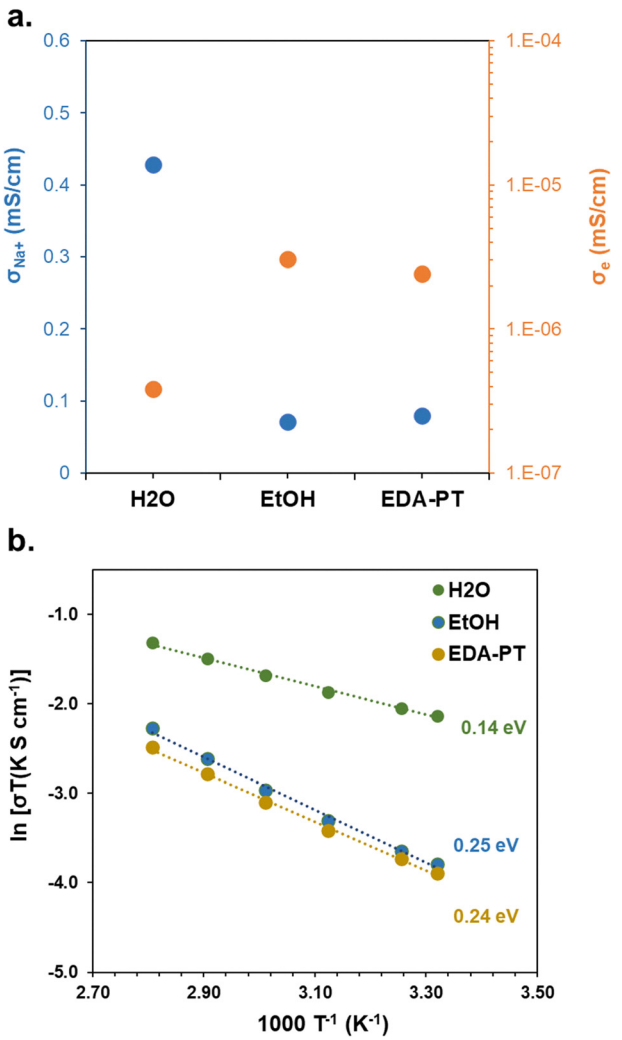

Fig. 5 (a) Ionic and electronic conductivity, and (b) Arrhenius plots of NSnSbS obtained from H_2O, EtOH, and EDA-PT solvents, and further annealed at 550 °C.

Detailed descriptions of the reactions involved are provided in the Experimental section. Further annealing of the recovered powder from aqueous and ethanolic solutions resulted in the decomposition of the material into elemental and binary compounds.

To facilitate Sn incorporation, we turned to the use of amine–thiol solvents. Our previous work has demonstrated that amine–thiol solvents are particularly effective for synthesizing Na_3SbSe_4 by activating selenium through a redox process. The use of amine–thiol co-solvents allows for the dissolution of highly insoluble selenium at high concentrations, generating homogeneous inks suitable for the solution processing of inorganic semiconductors.[66,67] In this process, an amine–thiol mixture produces highly reactive ammonium ions and thiolate species. The thiolate formation reduces Se to its anion form, while the complexation of selenium with ammonium ion yields soluble selenium in the form of $[(Se^{-2})(R\text{-}NH_3^+)_2]$. Furthermore, this solvent combination has been shown to effectively dissolve a wide range of binary selenides, such as Sb_2Se_3[64,68,69] and SnSe.[70,71] Inspired by these studies, we attempted the NSnSbSe synthesis in EDA-PT (4 : 1 v/v) with the following stoichiometry:

$$22Na_{(sol)} + Sb_2Se_{3(sol)} + 4SnSe_{2(sol)} + 11Se_{(sol)} \rightarrow 2Na_{11}Sn_2SbSe_{12(sol)} \quad (9)$$

Fig. 6a displays the XRD patterns of NSnSbSe recovered from EDA-PT by drying at 150 °C. The predominant phase of NSnSbSe with considerable Na_3SbSe_4 secondary phase was observed. Upon annealing the sample at 550 °C, we found that the ternary phase incorporates into the quaternary phase through a solid-state reaction. However, attempts to anneal the sample at temperatures exceeding 550 °C led to significant evaporation of selenium species and melting of the material, complicating sample collection. To facilitate high-temperature reactions, melt-quenching techniques using enclosed quartz containers are required.

The Raman spectra of the synthesized selenide at 150 °C and 550 °C are compared with those of the parent ternary compounds, Na_4SnSe_4 and Na_3SbSe_4, in Fig. 6b. The Na_3SbSe_4 is produced through the reaction of Sb_2Se_3 with sodium and selenium dissolved in EDA-PT solvents, as detailed in our previous work.[31] Similarly, the reaction involving $SnSe_2$, sodium, and selenium results in the formation of highly pure Na_4SnSe_4. The NSnSbSe compound exhibits strong Raman peaks at 197 and 230 cm^{-1}, which correspond to the vibrations of the Sn–Se bond, similar to those observed in other selenostannates such as Ba_2SnSe_4.[72,73] The peaks at 206, 259, and 271 are attributed to the stretching modes of $SbSe_4$ tetrahedra, as seen in the Na_3SbSe_4 spectrum, which closely resembles other compounds like K_3SbSe_4.[31,74]

The samples exhibit all the characteristic peaks associated with $[Sn/Sb]Se_4$ polyhedra, further confirming the successful formation of the quaternary phase. Consistent with the behavior observed in NSnSbS, the signature peak of $SbSe_4$ at 207 cm^{-1} shifts to a higher wavenumber (~212 cm^{-1}) upon annealing, indicating effective incorporation of Sb into the lattice structure. This trend is also noted for other vibrational modes of $SbSe_4$, reinforcing the notion of structural modifications upon thermal treatment.

However, the uncorrected full spectrum reveals the presence of D and G bands, which are indicative of carbonaceous species formed during solvent removal, even at low-temperature drying (Fig. S11, ESI†). This presence of carbonaceous material is likely contributing to the elevated electronic conductivity observed for NSnSbSe, as shown in Fig. S12 (ESI†). EIS analysis indicates that the 550 °C sample achieves an ionic conductivity (σ_{Na^+}) of 0.07 mS cm^{-1} and an activation energy (E_a) of 0.22 eV, which are considerably lower than those observed in other quaternary phases. This reduction can be attributed to the significant presence of the Na_3SbSe_4 secondary phase within the material. Previous attempts at the solid-state reaction of $Na_{11}Sn_2SbSe_{12}$ resulted in a substantial impurity phase of $NaSbSe_2$, which negatively impacted its ionic properties, yielding an ionic conductivity of 0.15 mS cm^{-1}.[3] Despite the presence of

© 2025 The Author(s). Published by the Royal Society of Chemistry

Open Access Article. Published on 02 July 2025. Downloaded on 5/21/2026 10:57:09 PM.
This article is licensed under a Creative Commons Attribution-NonCommercial 3.0 Unported Licence.

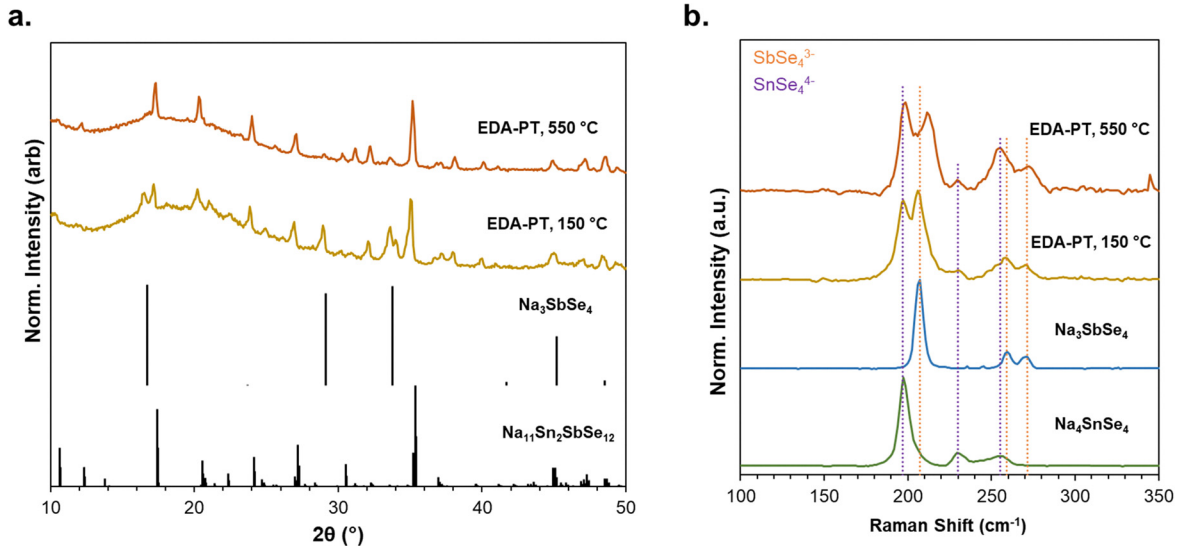

Fig. 6 (a) XRD, and (b) Raman of NSnSbSe recovered from amine–thiol solvents after annealing at 150 and 550 °C, respectively.

carbonaceous impurities, the current work represents the first liquid-based synthesis of quaternary selenide materials, to our knowledge. This pioneering approach could open new avenues for the development of high-performance solid-state electrolytes. Fig. S12 (ESI†) and Table 1 summarize the preparation conditions and transport properties of $Na_{11}PnCh_{12}$ (Pn = P, Sb; Ch = S, Se) produced in this work.

For the P-based selenide, the solution approach is highly challenging due to the extreme hygroscopic nature of white phosphorus (P_4). While red phosphorus serves as a more stable alternative, it is difficult to activate in organic solvents. Strumolo *et al.*[75] recently reported that red phosphorus can dissolve in an amine–thiol mixture, forming primarily cage-like polyphosphide anions (P_{16}^{2-}). However, our attempts to utilize these polyphosphides in EDA-PT were unsuccessful, as significant portion of dissolved phosphorus precipitated out of the solvent mixture. The Raman analysis of the obtained supernatant (Fig. S13, ESI†) closely matched ternary Na_4SnSe_4, suggesting that phosphorus remained unreactive in these reactions, likely due to steric effects associated with the polyphosphide structure.

Electrochemical performance of quaternary chalcogenides

We assessed the electrochemical stability window as-synthesized quaternary compounds using linear sweep voltammetry (LSV) in a Na–Sn|SSE|SS-SSE cell configuration at room temperature, with a scan rate of 0.1 mV s^{-1}. As shown in Fig. 7a, NSnSbS exhibits a wide electrochemical stability window, with reduction and oxidation processes occurring around 0.95 V and 2.9 V *vs.* Na–Sn alloy, respectively. A similar potential range was reported by Weng *et al.* through cyclic voltammetry, though the discrepancy in the low redox potential may stem from

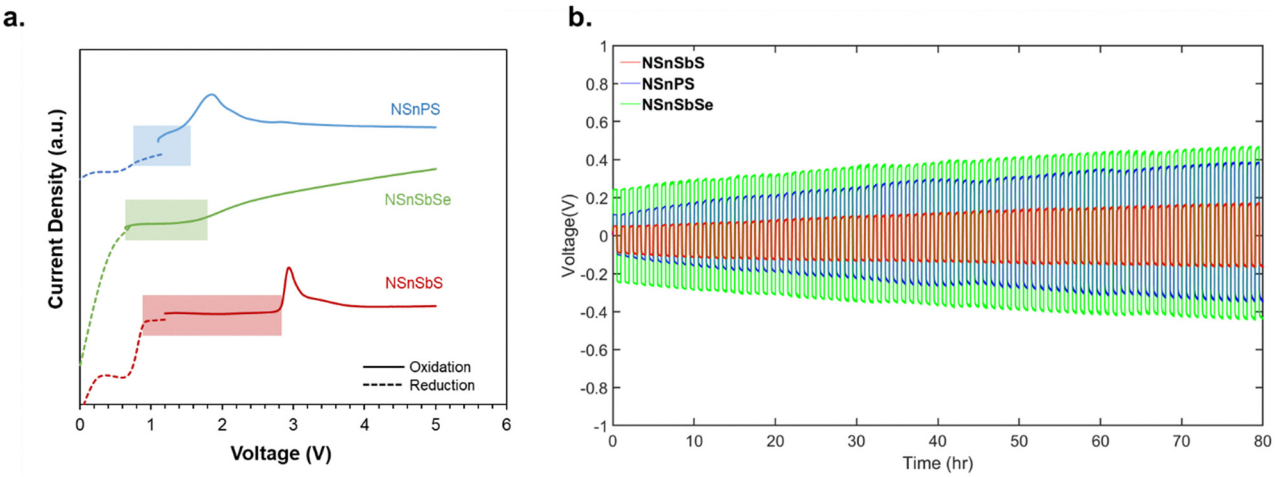

Fig. 7 (a) Linear sweep voltammetry of $Na_{11}Sn_2PnCh_{12}$ (Pn = P, Sb; Ch = S, Se) cells with a voltage range of 0–5 V at a scan rate of 0.1 mV s^{-1}, and (b) cyclability of Na–Sn|$Na_{11}Sn_2PCh_{12}$|Na–Sn symmetric cells at RT with a stacking pressure of 50 MPa.

Open Access Article. Published on 02 July 2025. Downloaded on 5/21/2026 10:57:09 PM. This article is licensed under a Creative Commons Attribution-NonCommercial 3.0 Unported Licence.

differences in establishing faradaic current onset in voltammetry data.[76] In contrast, NSnPS and NSnSbSe exhibit narrower stability windows of approximately 0.75–1.5 V and 0.65–1.8 V, respectively. Given the Na–Sn alloy potential of 0.2 V *vs.* Na^+/Na, the updated stability windows are summarized in Table 1. To our knowledge, NSnSbSe's electrochemical stability has not been previously reported. Selenides appear more susceptible to oxidation than their sulfide counterparts at elevated potentials resulting a smaller electrochemical stability as observed in other selenide systems such as selenophosphate-based lithium argyrodites.[77]

We also assembled symmetric Na–Sn|SSE|Na–Sn cells to evaluate the stability of the anode-solid electrolyte interface. As shown in Fig. 7b, NSnSbS exhibited the lowest initial overpotential of 50 mV, which gradually increased to ~169 mV over 90 hours of cycling. In contrast, NSnPS and NSnSbSe displayed significantly higher overpotentials of ~400 mV and ~470 mV, respectively. The transport property measurements (as shown in Fig. S13, ESI† and summarized in Table 1) confirm that aqueous-derived NSnSbS is the most suitable separator for Na all-solid-state batteries, owing to its high ionic conductivity, low electronic conductivity, and low activation barrier.

Conclusions

In conclusion, we presented the rational design of methods for the synthesis of quaternary chalcogenide solid-state electrolytes, $Na_{11}Sn_2PnCh_{12}$ (Pn = P, Sb; Ch = S, Se), using aprotic, protic, and alkahest solvents. The synthesis of P-containing quaternary is more complex due to the limited inventory of phosphorus reagents. Specifically, the high reactivity of P_2S_5 led us to use acetonitrile (ACN) with a high dielectric constant to ensure intimate mixing of the precursors, forming amorphous thiophosphate moieties, which were then converted to $Na_{11}Sn_2S_{12}$ through annealing. We found that heat-treatment at 300 °C is necessary to initiate the quaternary phase formation in this system, while higher temperatures (550 °C) are required to obtain phase pure $Na_{11}Sn_2PS_{12}$ with minimal Na_4SnS_4 impurity. For Sb-based analogs, polar solvents such as water, ethanol, and amine–thiol cosolvents facilitated the reaction and crystallization of $Na_{11}Sn_2SbS_{12}$ at a low temperature of 150 °C, with additional annealing needed to further enhance transport properties. The aqueous-recovered sample produced Na-based chalcogenides with performance comparable to that of energy-intensive, high-temperature solid-state reactions. Notably, we achieved the first liquid-phase synthesis of $Na_{11}Sn_2SbSe_{12}$ in this work, despite the presence of minor impurities. Overall, our findings demonstrate the potential of liquid-phase methods for the development of quaternary chalcogenides, offering advantages in achieving high ionic conductivity and phase purity, and paving the way for scalable production of Na-based solid-state electrolytes.

Author contributions

The manuscript was written through the contributions of all authors. All authors have approved the final version of the manuscript.

Conflicts of interest

There are no conflicts to declare.

Data availability

The data supporting this article have been included as part of the ESI.†

Acknowledgements

This work was supported by the National Science Foundation through Award 2219184. Some of the work was performed in the following core facility, which is a part of Colorado School of Mines' Shared Instrumentation Facility (X-ray Diffraction & Computed Tomography: RRID: SCR_022053, Scanning Probe and Optical Microscopy: RRID: SCR_022048).

References

1 H. Jia, L. Peng, C. Yu, L. Dong, S. Cheng and J. Xie, Chalcogenide-based inorganic sodium solid electrolytes, *J. Mater. Chem. A*, 2021, **9**, 5134–5148.
2 Z. Yang, B. Tang, D. Ren, X. Yu, Y. Gao, Y. Wu, Y. Yang, Z. Chen and Z. Zhou, Advancing solid-state sodium batteries: Status quo of sulfide-based solid electrolytes, *Mater. Today*, 2024, **80**, 429–449.
3 E. P. Ramos, A. Assoud, L. Zhou, A. Shyamsunder, D. Rettenwander and L. F. Nazar, Structure–transport correlations in $Na_{11}Sn_2SbSe_{12}$ and its sulfide solid solutions, *APL Mater.*, 2023, **11**, 011104.
4 S. K. Vineeth, M. Tebyetekerwa, H. Liu, C. B. Soni, N. Sungjemmenla, X. S. Zhao and V. Kumar, Progress in the development of solid-state electrolytes for reversible room-temperature sodium-sulfur batteries, *Mater. Adv.*, 2022, **2**, 6415–6440.
5 F. Tsuji, A. Nasu, C. Hotehama, A. Sakuda, M. Tatsumisago and A. Hayashi, Preparation and characterization of sodium-ion conductive Na3BS3 glass and glass–ceramic electrolytes, *Mater. Adv.*, 2021, **2**, 1676–1682.
6 S. Yubuchi, A. Hayashi and M. Tatsumisago, Sodium-ion conducting Na3PS4 electrolyte synthesized *via* a liquid-phase process using N-methylformamide, *Chem. Lett.*, 2015, **44**, 884–886.
7 A. Banerjee, K. H. Park, J. W. Heo, Y. J. Nam, C. K. Moon, S. M. Oh, S.-T. T. Hong and Y. S. Jung, Na_3SbS_4: A Solution Processable Sodium Superionic Conductor for All-Solid-State Sodium-Ion Batteries, *Angew. Chem., Int. Ed.*, 2016, **55**, 9634–9638.
8 L. Zhang, D. Zhang, K. Yang, X. Yan, L. Wang, J. Mi, B. Xu and Y. Li, Vacancy-Contained Tetragonal Na3SbS4 Superionic Conductor, *Adv. Sci.*, 2016, **3**, 1600089.
9 D. Zhang, X. Cao, D. Xu, N. Wang, C. Yu, W. Hu, X. Yan, J. Mi, B. Wen, L. Wang and L. Zhang, Synthesis of cubic Na3SbS4 solid electrolyte with enhanced ion transport for

© 2025 The Author(s). Published by the Royal Society of Chemistry

Open Access Article. Published on 02 July 2025. Downloaded on 5/21/2026 10:57:09 PM. This article is licensed under a Creative Commons Attribution-NonCommercial 3.0 Unported Licence.

all-solid-state sodium-ion batteries, *Electrochim. Acta*, 2018, **259**, 100–109.

10 H. Wang, Y. Chen, Z. D. Hood, G. Sahu, A. S. Pandian, J. K. Keum, K. An and C. Liang, An Air-Stable Na3SbS4 Superionic Conductor Prepared by a Rapid and Economic Synthetic Procedure, *Angew. Chem., Int. Ed.*, 2016, **55**, 8551–8555.

11 S. A. Vaselabadi, W. H. Smith and C. A. Wolden, Solution Synthesis of Sb2S3 and Na3SbS4 Solid-State Electrolyte, *J. Electrochem. Soc.*, 2021, **168**, 110533.

12 S. H. Bo, Y. Wang, J. C. Kim, W. D. Richards and G. Ceder, Computational and Experimental Investigations of Na-Ion Conduction in Cubic Na_3PSe_4, *Chem. Mater.*, 2016, **28**, 252–258.

13 T. Krauskopf, C. Pompe, M. A. Kraft and W. G. Zeier, Influence of Lattice Dynamics on Na^+ Transport in the Solid Electrolyte $Na_3PS_{4-x}Se_x$, *Chem. Mater.*, 2017, **29**, 8859–8869.

14 Z. Zhang, E. Ramos, F. Lalère, A. Assoud, K. Kaup, P. Hartman and L. F. Nazar, $Na_{11}Sn_2PS_{12}$: A new solid state sodium superionic conductor, *Energy Environ. Sci.*, 2018, **11**, 87–93.

15 M. Duchardt, U. Ruschewitz, S. Adams, S. Dehnen and B. Roling, Vacancy-Controlled Na^+ Superion Conduction in $Na_{11}Sn_2PS_{12}$, *Angew. Chem., Int. Ed.*, 2018, **57**, 1351–1355.

16 A. Tiwari, S. K. Singh, N. Srivastava, D. Meghnani, R. Mishra, R. K. Tiwari, A. Patel, H. Gupta, V. K. Tiwari and R. K. Singh, Diffusion mechanism in a sodium superionic sulfide-based solid electrolyte: $Na_{11}Sn_2AsS_{12}$, *J. Phys. D: Appl. Phys.*, 2022, **55**, 355503.

17 T. Fuchs, S. P. Culver, P. Till and W. G. Zeier, Defect-Mediated Conductivity Enhancements in $Na_{3-x}Pn_{1-x}W_xS_4$ (Pn = P, Sb) Using Aliovalent Substitutions, *ACS Energy Lett.*, 2020, **5**, 146–151.

18 V. S. Kandagal, M. D. Bharadwaj and U. V. Waghmare, Theoretical prediction of a highly conducting solid electrolyte for sodium batteries: $Na_{10}GeP_2S_{12}$, *J. Mater. Chem. A*, 2015, **3**, 12992–12999.

19 W. D. Richards, T. Tsujimura, L. Miara, Y. Wang, J. C. Kim, S. P. Ong, I. Uechi, N. Suzuki and G. Ceder, Design and synthesis of the superionic conductor $Na_{10}SnP_2S_{12}$-SI, *Nat. Commun.*, 2016, **5**, 10–13.

20 E. P. Ramos, Z. Zhang, A. Assoud, K. Kaup, F. Lalère and L. F. Nazar, Correlating Ion Mobility and Single Crystal Structure in Sodium-Ion Chalcogenide-Based Solid State Fast Ion Conductors: $Na_{11}Sn_2PnS_{12}$ (Pn = Sb, P), *Chem. Mater.*, 2018, **30**, 7413–7417.

21 J. W. Heo, A. Banerjee, K. H. Park, Y. S. Jung and S. T. Hong, New Na-Ion Solid Electrolytes $Na_{4-x}Sn_{1-x}Sb_xS_4$ ($0.02 \leq x \leq 0.33$) for All-Solid-State Na-Ion Batteries, *Adv. Energy Mater.*, 2018, **8**, 4–9.

22 M. Duchardt, S. Neuberger, U. Ruschewitz, T. Krauskopf, W. G. Zeier, J. Schmedt auf der Günne, S. Adams, B. Roling and S. Dehnen, Superion Conductor $Na_{11.1}Sn_{2.1}P_{0.9}Se_{12}$: Lowering the Activation Barrier of Na^+ Conduction in Quaternary 1–4–5–6 Electrolytes, *Chem. Mater.*, 2018, **30**, 4134–4139.

23 M. Ghidiu, J. Ruhl, S. P. Culver and W. G. Zeier, Solution-based synthesis of lithium thiophosphate superionic conductors for solid-state batteries: A chemistry perspective, *J. Mater. Chem. A*, 2019, **7**, 17735–17753.

24 J. Xu, L. Liu, N. Yao, F. Wu, H. Li and L. Chen, Liquid-involved synthesis and processing of sulfide-based solid electrolytes, electrodes, and all-solid-state batteries, *Mater. Today Nano*, 2019, **8**, 100048.

25 J. E. Lee, K. H. Park, J. C. Kim, T. U. Wi, A. R. Ha, Y. B. Song, D. Y. Oh, J. Woo, S. H. Kweon, S. J. Yeom, W. Cho, K. S. Kim, H. W. Lee, S. K. Kwak and Y. S. Jung, Universal Solution Synthesis of Sulfide Solid Electrolytes Using Alkahest for All-Solid-State Batteries, *Adv. Mater.*, 2022, **2200083**, 1–11.

26 Z. Warren and N. C. Rosero-Navarro, Solution-Based Suspension Synthesis of Li_2S–P_2S_5 Glass-Ceramic Systems as Solid-State Electrolytes: A Brief Review of Current Research, *ACS Omega*, 2024, **9**, 31228–31236.

27 T. W. Kim, K. H. Park, Y. E. Choi, J. Y. Lee and Y. S. Jung, Aqueous-solution synthesis of Na_3SbS_4 solid electrolytes for all-solid-state Na-ion batteries, *J. Mater. Chem. A*, 2018, **6**, 840–844.

28 F. Hartmann, A. Benkada, S. Indris, M. Poschmann, H. Lühmann, P. Duchstein, D. Zahn and W. Bensch, Directed dehydratation as synthetic tool for generation of a new Na_4SnS_4 polymorph: Crystal structure, Na^+ conductivity, and influence of Sb-substitution, *Angew. Chem., Int. Ed.*, 2022, **61**, e202202182.

29 W. Weng, H. Wan, G. Liu, L. Wu, J. Wu and X. Yao, Liquid-Phase Synthesis of Nanosized $Na_{11}Sn_2PS_{12}$ Solid Electrolytes for Room Temperature All-Solid-State Sodium Batteries, *ACS Appl. Energy Mater.*, 2021, **4**, 1467–1473.

30 W. H. Smith, J. Birnbaum and C. A. Wolden, Production and purification of anhydrous sodium sulfide, *J. Sulfur Chem.*, 2021, **42**, 426–442.

31 S. A. Vaselabadi, K. Palmer, W. H. Smith and C. A. Wolden, Scalable Synthesis of Selenide Solid-State Electrolytes for Sodium-Ion Batteries, *Inorg. Chem.*, 2023, **62**, 17102–17114.

32 S. Chandrasekaran, L. Yao, L. Deng, C. Bowen, Y. Zhang, S. Chen, Z. Lin, F. Peng and P. Zhang, Recent advances in metal sulfides: From controlled fabrication to electrocatalytic, photocatalytic and photoelectrochemical water splitting and beyond, *Chem. Soc. Rev.*, 2019, **48**, 4178–4280.

33 J. Yu, C. Y. Xu, F. X. Ma, S. P. Hu, Y. W. Zhang and L. Zhen, Monodisperse SnS_2 nanosheets for high-performance photocatalytic hydrogen generation, *ACS Appl. Mater. Interfaces*, 2014, **6**, 22370–22377.

34 W. Fu, J. Wang, S. Zhou, R. Li and T. Peng, Controllable Fabrication of Regular Hexagon-Shaped SnS_2 Nanoplates and Their Enhanced Visible-Light-Driven H2 Production Activity, *ACS Appl. Nano Mater.*, 2018, **1**, 2923–2933.

35 F. Zhang, C. Xia, J. Zhu, B. Ahmed, H. Liang, D. B. Velusamy, U. Schwingenschlögl and H. N. Alshareef, SnSe2 2D Anodes for Advanced Sodium Ion Batteries, *Adv. Energy Mater.*, 2016, **6**, 1601188.

36 T. Wang, K. Yang, J. Shi, S. Zhou, L. Mi, H. Li and W. Chen, Simple synthesis of sandwich-like $SnSe_2$/rGO as high initial

Open Access Article. Published on 02 July 2025. Downloaded on 5/21/2026 10:57:09 PM. This article is licensed under a Creative Commons Attribution-NonCommercial 3.0 Unported Licence.

coulombic efficiency and high stability anode for sodium-ion batteries, *J. Energy Chem.*, 2020, **46**, 71–77.

37 W. Feng, M. Cheng, R. Du, Y. Wang, P. Wang, H. Li, L. Song, X. Wen, J. Yang, X. Li, J. He and J. Shi, Gram-Scale Synthesized Two-Dimensional VSe_2 and $SnSe_2$ for Ultrahigh Electrocatalytic Sulfion Recycling, *Adv. Mater. Interfaces*, 2022, **9**, 2200060.

38 P. Ramasamy, P. Manivasakan and J. Kim, Phase controlled synthesis of SnSe and $SnSe_2$ hierarchical nanostructures made of single crystalline ultrathin nanosheets, *CrystEngComm*, 2015, **17**, 807–813.

39 J. Choi, J. Jin, I. G. Jung, J. M. Kim, H. J. Kim and S. U. Son, $SnSe_2$ nanoplate–graphene composites as anode materials for lithium ion batteries, *Chem. Commun.*, 2011, **47**, 5241–5243.

40 S. Saha, A. Banik and K. Biswas, Few-Layer Nanosheets of n-Type $SnSe_2$, *Chem. – Eur. J.*, 2016, **22**, 15634–15638.

41 G. Lindberg, A. Larsson, M. Råberg, D. Boström, R. Backman and A. Nordin, Determination of thermodynamic properties of Na_2S using solid-state EMF measurements, *J. Chem. Thermodyn.*, 2007, **39**, 44–48.

42 H. Gamsjäger, J. Sangster and S. K. Saxena, *CHEMICAL THERMODYNAMICS OF TIN Tamás GAJDA*.

43 S. A. Vaselabadi, B. Benham and C. A. Wolden, Facile one-pot synthesis of high-purity sodium antimony chalcogenides in polar solvents, *Inorg. Chem. Front.*, 2025, **12**, 658–671.

44 C. Wang, K. Tang, Q. Y. Aa and Y. Qian, Raman scattering, far infrared spectrum and photoluminescence of SnS_2 nanocrystallites, *Chem. Phys. Lett.*, 2002, **357**, 371–375.

45 S. H. Choi, W. J. Kim, B. H. Lee, S. C. Kim, J. G. Kang and D. W. Kim, Rational design of one-pot solvent-assisted synthesis for multi-functional Sn-substituted superionic Li argyrodite solid electrolytes, *J. Mater. Chem. A*, 2023, **11**, 14690–14704.

46 M. Uematsu, S. Yubuchi, F. Tsuji, A. Sakuda, A. Hayashi and M. Tatsumisago, Suspension synthesis of $Na_{3-x}PS_{4-x}Cl$ solid electrolytes, *J. Power Sources*, 2019, **428**, 131–135.

47 H. Wan, J. P. Mwizerwa, X. Qi, X. Xu, H. Li, Q. Zhang, L. Cai, Y.-S. Hu and X. Yao, Nanoscaled Na_3PS_4 Solid Electrolyte for All-Solid-State FeS_2/Na Batteries with Ultrahigh Initial Coulombic Efficiency of 95% and Excellent Cyclic Performances, *ACS Appl. Mater. Interfaces*, 2018, **10**, 12300–12304.

48 M. Uematsu, S. Yubuchi, K. Noi, A. Sakuda, A. Hayashi and M. Tatsumisago, Preparation of Na_3PS_4 electrolyte by liquid-phase process using ether, *Solid State Ionics*, 2018, **320**, 33–37.

49 H. Wan, J. P. Mwizerwa, X. Qi, X. Liu, X. Xu, H. Li, Y.-S. Hu and X. Yao, Core–Shell $Fe_{1-x}S@Na_{2.9}PS_{3.95}Se_{0.05}$ Nanorods for Room Temperature All-Solid-State Sodium Batteries with High Energy Density, *ACS Nano*, 2018, **12**, 2809–2817.

50 M. Olson, J. Wheaton, M. Okkema, N. Oldham and S. W. Martin, Optimized Thin Film Processing of Sodium Mixed Oxy-Sulfide-Nitride Glassy Solid Electrolytes for All-Solid-State Batteries, *ACS Appl. Energy Mater.*, 2023, **6**, 5842–5855.

51 T. Scholz, C. Schneider, R. Eger, V. Duppel, I. Moudrakovski, A. Schulz, J. Nuss and B. V. Lotsch, Phase formation through synthetic control: polymorphism in the sodium-ion solid electrolyte $Na_4P_2S_6$, *J. Mater. Chem. A*, 2021, **9**, 8692–8703.

52 T. Famprikis, H. Bouyanfif, P. Canepa, M. Zbiri, J. A. Dawson, E. Suard, F. Fauth, H. Y. Playford, D. Dambournet, O. J. Borkiewicz, M. Courty, O. Clemens, J.-N. Chotard, M. S. Islam and C. Masquelier, Insights into the Rich Polymorphism of the Na^+ Ion Conductor Na_3PS_4 from the Perspective of Variable-Temperature Diffraction and Spectroscopy, *Chem. Mater.*, 2021, **33**, 5652–5667.

53 X. Chi, Y. Zhang, F. Hao, S. Kmiec, H. Dong, R. Xu, K. Zhao, Q. Ai, T. Terlier, L. Wang, L. Zhao, L. Guo, J. Lou, H. L. Xin, S. W. Martin and Y. Yao, An electrochemically stable homogeneous glassy electrolyte formed at room temperature for all-solid-state sodium batteries, *Nat. Commun.*, 2022, **13**, 2854.

54 C. Dietrich, D. A. Weber, S. Culver, A. Senyshyn, S. J. Sedlmaier, S. Indris, J. Janek and W. G. Zeier, Synthesis, Structural Characterization, and Lithium Ion Conductivity of the Lithium Thiophosphate $Li_2P_2S_6$, *Inorg. Chem.*, 2017, **56**, 6681–6687.

55 A. Benkada, F. Hartmann, M. Poschmann, S. Indris, H. Lühmann and W. Bensch, Directed Dehydration of $Na_4Sn_2S_6{\cdot}5H_2O$ Generates the New Compound $Na_4Sn_2S_6$: Crystal Structure and Selected Properties, *Eur. J. Inorg. Chem.*, 2023, 6–11.

56 A. Benkada, F. Hartmann, T. A. Engesser, S. Indris, T. Zinkevich, C. Näther, H. Lühmann, H. Reinsch, S. Adams and W. Bensch, Room-Temperature Solid-State Transformation of $Na_4SnS_4{\cdot}14H_2O$ into $Na_4Sn_2S_6{\cdot}5H_2O$: An Unusual Epitaxial Reaction Including Bond Formation, Mass Transport, and Ionic Conductivity, *Chem. – Eur. J.*, 2023, **29**, e202202318.

57 M. Duchardt, S. Neuberger, U. Ruschewitz, T. Krauskopf, W. G. Zeier, J. Schmedt auf der Günne, S. Adams, B. Roling and S. Dehnen, Superion Conductor $Na_{11.1}Sn_{2.1}P_{0.9}Se_{12}$: Lowering the Activation Barrier of Na^+ Conduction in Quaternary 1–4–5–6 Electrolytes, *Chem. Mater.*, 2018, **30**, 4134–4139.

58 Z. Yu, S. L. Shang, D. D. Wang, Y. C. Li, H. P. Yennawar, G. Li, H.-T. T. Huang, Y. Gao, T. E. Mallouk, Z.-K. K. Liu and D. D. Wang, Synthesis and understanding of $Na_{11}Sn_2PSe_{12}$ with enhanced ionic conductivity for all-solid-state Na-ion battery, *Energy Storage Mater.*, 2019, **17**, 70–77.

59 R. P. Rao, X. Zhang, K. C. Phuah and S. Adams, Mechanochemical synthesis of fast sodium ion conductor $Na_{11}Sn_2PSe_{12}$ enables first sodium-selenium all-solid-state battery, *J. Mater. Chem. A*, 2019, **7**, 20790–20798.

60 S. D. Deshmukh, L. F. Easterling, J. M. Manheim, N. J. Libretto, K. G. Weideman, J. T. Miller, H. I. Kenttämaa and R. Agrawal, Analyzing and tuning the chalcogen-amine-thiol complexes for tailoring of chalcogenide syntheses, *Inorg. Chem.*, 2020, **59**, 8240–8250.

61 W. Schiwy, S. Pohl and B. Krebs, Darstellung und Struktur von Na_4SnS_4 - 14 H_2O, *J. Inorg. Gen. Chem.*, 1973, **402**, 77–86.

© 2025 The Author(s). Published by the Royal Society of Chemistry

Open Access Article. Published on 02 July 2025. Downloaded on 5/21/2026 10:57:09 PM. This article is licensed under a Creative Commons Attribution-NonCommercial 3.0 Unported Licence.

62 Y. Oh, S. Bag, C. D. Malliakas and M. G. Kanatzidis, Selective surfaces: High-surface-area zinc tin sulfide chalcogels, *Chem. Mater.*, 2011, **23**, 2447–2456.
63 P. D. Antunez, D. A. Torelli, F. Yang, F. A. Rabuffetti, N. S. Lewis and R. L. Brutchey, Low Temperature Solution-Phase Deposition of SnS Thin Films, *Chem. Mater.*, 2014, **26**, 5444–5446.
64 D. H. Webber and R. L. Brutchey, Alkahest for V2VI3 chalcogenides: Dissolution of nine bulk semiconductors in a diamine-dithiol solvent mixture, *J. Am. Chem. Soc.*, 2013, **135**, 15722–15725.
65 W. Mikenda and A. Preisinger, Vibrational spectra of Na_3SbS_4, $Na_3SbS_4{\cdot}9H_2O$ (Schlippe's salt) and $Na_3SbS_4{\cdot}9D_2O$, *Spectrochim. Acta, Part A*, 1980, **36**, 365–370.
66 B. C. Walker and R. Agrawal, Contamination-free solutions of selenium in amines for nanoparticle synthesis, *Chem. Commun.*, 2014, **50**, 8331–8334.
67 D. H. Webber, J. J. Buckley, P. D. Antunez and R. L. Brutchey, Facile dissolution of selenium and tellurium in a thiol-amine solvent mixture under ambient conditions, *Chem. Sci.*, 2014, **5**, 2498–2502.
68 A. Vashishtha, O. Vana and E. Edri, Solvent composition regulates the Se:Sb ratio in antimony selenide nanowires deposited from thiol-amine solvent mixtures, *Nanoscale Adv.*, 2022, **4**, 772–781.
69 C. L. McCarthy, D. H. Webber, E. C. Schueller and R. L. Brutchey, Solution-Phase Conversion of Bulk Metal Oxides to Metal Chalcogenides Using a Simple Thiol-Amine Solvent Mixture, *Angew. Chem., Int. Ed.*, 2015, **54**, 8378–8381.
70 R. Zhang, S. Cho, D. G. Lim, X. Hu, E. A. Stach, C. A. Handwerker and R. Agrawal, Metal-metal chalcogenide molecular precursors to binary, ternary, and quaternary metal chalcogenide thin films for electronic devices, *Chem. Commun.*, 2016, **52**, 5007–5010.
71 C. L. McCarthy and R. L. Brutchey, Preparation of electrocatalysts using a thiol-amine solution processing method, *Dalton Trans.*, 2018, **47**, 5137–5143.
72 L. Gao, G. Bian, Y. Yang, B. Zhang, X. Wu and K. Wu, Na_4SnS_4 and Na_4SnSe_4 exhibiting multifunctional physicochemical performances as potential infrared nonlinear optical crystals and sodium ion conductors, *New J. Chem.*, 2021, **45**, 12362–12366.
73 K. Wu, X. Su, Z. Yang and S. Pan, An investigation of new infrared nonlinear optical material: $BaCdSnSe_4$, and three new related centrosymmetric compounds: Ba_2SnSe_4, Mg_2GeSe_4, and $Ba_2Ge_2S_6$, *Dalton Trans.*, 2015, **44**, 19856–19864.
74 N. Ding, Y. Takabayashi, P. L. Solari, K. Prassides, R. J. Pcionek and M. G. Kanatzidis, Cubic gyroid frameworks in mesostructured metal selenides created from tetrahedral Zn^{2+}, Cd^{2+}, and in 3^+ ions and the $[SbSe_4]$ 3- precursor, *Chem. Mater.*, 2006, **18**, 4690–4699.
75 M. J. Strumolo, D. B. Eremin, S. Wang, C. Mora Perez, O. V. Prezhdo, J. S. Figueroa and R. L. Brutchey, Formation of a P162- Ink from Elemental Red Phosphorus in a Thiol-Amine Mixture, *Inorg. Chem.*, 2023, **62**, 6197–6201.
76 W. Weng, G. Liu, L. Shen and X. Yao, High ionic conductivity and stable phase $Na_{11.5}Sn_2Sb_{0.5}Ti_{0.5}S_{12}$ for all-solid-state sodium batteries, *J. Power Sources*, 2021, **512**, 230485.
77 J. Hartel, A. Banik, J. M. Gerdes, B. Wankmiller, B. Helm, C. Li, M. A. Kraft, M. R. Hansen and W. G. Zeier, Understanding Lithium-Ion Transport in Selenophosphate-Based Lithium Argyrodites and Their Limitations in Solid-State Batteries, *Chem. Mater.*, 2023, **35**, 4798–4809.